Prediction of noise from a wing-in-junction flow using computational fluid dynamics

Con J. Doolan, Jesse L. Coombs, Danielle J. Moreau, Anthony C. Zander and Laura A. Brooks

School of Mechanical Engineering, University of Adelaide, Australia

ABSTRACT

The leading edge turbulence interaction noise model of Amiet was extended to incorporate span-wise variations in flow properties and integration with modern computational fluid dynamics codes. The present implementation of the leading edge noise model was validated against experimental data in the literature. To demonstrate the use of the extended leading edge noise model, the flow and noise from a wing-in-junction test case was simulated numerically. Noise was calculated using flow data from different upstream positions to illustrate the importance of choosing the most appropriate turbulence data for noise prediction. The effect of span-wise discretisation on the acoustic prediction was shown and a study of the noise contributions from each span-wise part of the wing was performed. This showed that the upper part of the wing produced the most noise. Thus, any noise mitigation strategies should be concentrated in this area for maximum effect.

INTRODUCTION

The interaction of turbulent flow with an airfoil creates unsteady lift, which is a source of broadband noise. This type of noise, known as turbulence leading edge interaction noise, is important for many applications, such as wind turbine rotors encountering turbulent gusts, helicopter rotors interacting with turbulence from preceding blade wakes and gas turbine compressor blades that pass through areas of turbulent flow either from the atmosphere or from wakes created by other rotors or stators in compressor cascades. It is therefore important that the physics controlling this type of noise is understood completely and methods are available for engineers to accurately predict it.

Figure 1 illustrates the essential components of turbulence leading edge interaction noise (known as leading edge noise hereafter). Turbulent eddies with characteristic length scale L (created by atmospheric shear, a wall boundary layer or by other components upstream of the airfoil) are convected toward an airfoil by the flow. When the eddies reach the leading edge, the random velocity fluctuations in the flow induce an unsteady pressure over the surface of the airfoil. The unsteady pressure distribution creates unsteady lift that, by the theory of Curle (1955), creates noise. This is a different mechanism to that found at the trailing edge (Moreau et al., 2011), where turbulent eddies created in the boundary layer produce noise via an edge diffraction process. In this paper, only leading-edge interaction noise is considered.

Most semi-analytical techniques that are used for the prediction of leading-edge noise are based on the theory of Amiet (1975). This is a very useful methodology and has been used by many researchers (Paterson & Amiet, 1982; Roger & Moreau, 2004); however, it was derived for cases where homogeneous turbulence encounters an airfoil or wing so the turbulence properties do not vary across the span. In many situations, this is not the case. For example, turbulent inflows may vary considerably across the radius of a wind turbine blade as it passes through different regions of the atmospheric boundary layer. It is therefore necessary to develop new prediction methodologies that can incorporate span-wise variations in flow properties. Moreover, it is advantageous to combine such a technique with modern computational fluid dynamics (CFD) that can predict the mean flow properties for use as an input to the noise model.

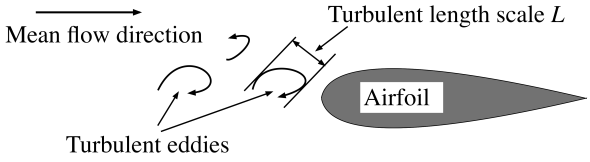

Figure 1. Side view of an airfoil encountering a turbulent flow field. When the turbulent eddies interact with the airfoil leading edge, unsteady lift is produced, which is a source of noise.

There are several methods of numerically simulating turbulent flow about an airfoil. However, the only practical method that can be used for engineering design is the solution of the Reynolds-averaged Navier-Stokes (RANS) equations. This is because other methods such as Large Eddy Simulation (LES) or Direct Numerical Simulation (DNS) require high computational resources and solution times, making them impractical for use in situations where multiple design solutions must be evaluated in a realistic time. For leading edge noise considerations, the use of RANS in the design process is to quantify and influence the flow properties upstream of an airfoil. For example, RANS can be used to calculate the flow properties in an air-conditioning duct in order to evaluate the noise created by a fan located within it.

The aim of this paper is to present a technique that links RANS flow solutions with a semi-analytical leading-edge noise prediction method. It is complementary to other meth-

ods currently under development at the University of Adelaide for other airfoil self noise mechanisms, such as trailing edge noise (Doolan et al., 2010). Additionally, this paper extends the leading-edge noise model so that it is able to accommodate span-wise variations in turbulent flow properties

The paper is structured as follows. The leading edge noise model is presented, including a description of how it can be used with a RANS flow solution and how to take into account span-wise variations in the flow. The noise model is then validated against published leading edge noise data for an airfoil placed in homogeneous turbulence to show that the described implementation of the model is accurate. Finally, the entire model is used on the complex flow demonstration test case of a wing-in-junction flow. Here, a RANS flow solution is presented and used to predict the noise in the far-field.

LEADING EDGE NOISE MODEL

Theory of Amiet

When unsteady flow (such as turbulence) encounters the leading edge of an airfoil, the airfoil experiences a fluctuating lift response, a side effect of which is a small component of the flow energy is radiated as sound to the far-field. Amiet (1975) has derived a model describing this sound generation process. This theory is based on a derivation of the cross-power-spectral density of surface pressure on the airfoil surface to far-field sound that uses the techniques of Curle (1955). Following this derivation gives the power spectral density for far-field noise, G_{pp}, generated by the interaction of turbulence with the leading edge of an airfoil.

$$G_{pp}(\mathbf{x},\omega) = 2d\left(\frac{z_a \rho_0 U_0}{\sigma^2}\right)^2 \left(\frac{\omega b}{c_0}\right)^2 |\mathcal{L}|^2 \phi_{ww}(\omega) l_y(\omega) \tag{1}$$

where $\mathbf{x} = (x_a, 0, z_a)$ is the observer position vector with respect to an origin at the mid-chord and mid-span of the airfoil and with x_a the chord-wise distance, y_a the span-wise distance and z_a the perpendicular distance (relative to the airfoil) to the observer. Other symbols are defined as follows: d is the half-span, b is the half-chord, ρ_0 is the ambient density of the fluid, U_0 is the mean free stream flow velocity, $\omega = 2\pi f$ is the angular frequency (f is the frequency in Hz) and c_0 is the speed of sound of the ambient fluid. The symbols $\phi_{ww}(\omega)$ and $l_y(\omega)$ relate to the vertical velocity turbulence spectrum and span-wise correlation length scale respectively. In this work, the Karman spectrum is used to define these quantities, full details of which are documented in Amiet (1975). The symbol σ is the far-field corrected distance, defined as

$$\sigma = \sqrt{x_a^2 + \beta^2 (y_a^2 + z_a^2)} \tag{2}$$

with the compressibility term defined as $\beta = \sqrt{1 - M^2}$, where M is the Mach number of the flow ($M = U_0/c_0$). The symbol $\mathcal{L}$ represents an airfoil response function that relates fluctuating lift to noise. The response function has solutions for low and high frequencies, as detailed by Amiet (1975). The low frequency solution is valid when $\frac{M\omega b}{U\beta^2} < \frac{\pi}{4}$ and the high frequency solution is valid for all other frequencies. The response function itself is lengthy to document, hence the reader is referred to Amiet (1975) for complete details.

Using RANS data as an input

When using a RANS simulation to provide turbulent inflow data for noise calculations, a method is needed to provide turbulence intensity and length scale to the noise model from the computed flow field.

Turbulence intensity (*TI*) can be calculated using (Wilcox, 2006)

$$TI = \sqrt{\frac{2}{3}\frac{k}{U^2}} \tag{3}$$

where k is the turbulent kinetic energy of the flow provided by the RANS simulation and U is the mean local velocity.

The turbulent integral length scale L can be determined using (Wilcox, 2006)

$$L = C^* \frac{k^{3/2}}{\epsilon} \tag{4}$$

where ϵ is the turbulent dissipation rate provided by the RANS simulation. The constant C^* is needed to relate the turbulence parameters to the length scale. Traditionally, a value of C^*=0.09 is used for this purpose (Wilcox, 2006). However, when this value is used with the RANS flow data, the turbulent length scale is much too small (much smaller than the boundary layer height), which is not realistic as it is expected that the maximum turbulent length scale should be similar to the boundary layer height (Pope, 2000). The under prediction of the length scale can be traced to an over prediction of turbulent dissipation by the RANS flow model. Based on a careful comparison of experimental flat plate boundary layer measurements and numerical simulation (a separate and as yet unpublished study), a value of C^*=10 was found to give the most realistic estimates of turbulent length scale and this will be used for the demonstration of the noise prediction method in this paper. Development of accurate turbulent length scale estimation methods from RANS flow data is an on-going area of research in this project.

Discretisation of the airfoil for noise calculations

The incoming flow will be non-uniform in many situations encountered in engineering design, such as wind turbines, propellors, ducted fans and for the present test case of a wing-in-junction flow. Figure 2 shows an idealised general example of span-wise varying turbulent flow with mean local velocity U encountering an airfoil. Figure 2 also shows a non-uniform turbulent length scale (L) across the span and a similar graph could be drawn showing a varying turbulent kinetic energy or turbulence intensity.

The theory of Amiet was developed for uniform turbulent inflow and must be modified to take into account span-wise varying turbulent conditions. The method proposed here is to discretise the span into many small segments of width dy, as

shown in Figure 2, and assume that the flow conditions are uniform across each strip. The noise from the airfoil is then a sum of contributions from each strip. If the airfoil is discretised into N strips, d$y = 2d/N$, and the total noise is

$$G_{pp,N} = \sum_{i=1}^{N} \frac{2d}{N} \left(\frac{z_{a,i} \rho_0 U_0}{\sigma_i^2} \right)^2 \left(\frac{\omega b}{c_0} \right)^2 |\mathcal{L}|^2 \phi_{ww,i}(\omega) l_{y,i}(\omega) \tag{5}$$

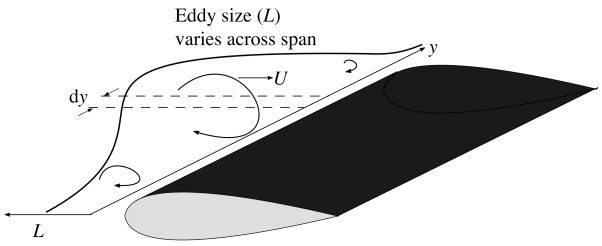

Figure 2. Airfoil encountering a turbulent flow with mean local velocity U that has varying properties across its span. The figure depicts the variation of turbulent integral length scale (L) across the airfoil's span. A strip of width dy is shown and this is used as part of the noise prediction method.

Validation of Amiet's Theory

The experimental results of Paterson and Amiet (1977) are used to validate the present implementation of Amiet's leading edge noise model, for the case of uniform span-wise turbulent flow. Here, a NACA 0012 airfoil with 0.23 m chord and 0.53 m span was placed in a homogeneous turbulent stream at zero angle of attack. The test case selected for comparison had a mean flow speed of 60 m/s and a turbulence intensity of 3.9%. The integral turbulence length scale L was 30 mm. Noise was measured using a microphone 2.25 m directly overhead the mid-chord of the airfoil. Full details of the tests can be found in Paterson and Amiet (1977).

For validation against theory, the high frequency airfoil response function was used. The Karman turbulence model was also used in the calculation. The results are compared in Figure 3 where theory predicts the experimental spectrum reasonably well. Above approximately 1500 Hz, the experimental results do not match the model. This is because (as discussed in Paterson and Amiet (1977)) the signal-to-noise ratio at these frequencies was poor.

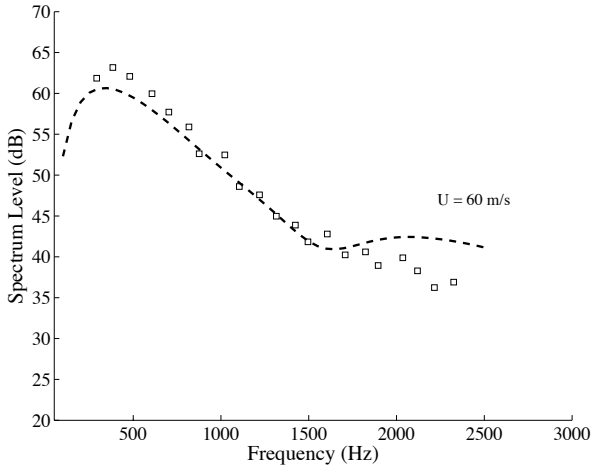

Figure 3. Comparison of the theory of Amiet with experimental results (Paterson & Amiet, 1977). The data shown are a 1 Hz bandwidth power spectrum, referenced to 20 μPa.

WING-IN-JUNCTION TEST CASE

Numerical Details

To demonstrate the leading-edge noise prediction method on a complex flow case, a wing-in-junction flow was simulated numerically. The flow geometry is shown in Figure 4. The airfoil (wing) shown in the figure has a NACA 0012 profile and was set at zero angle of attack. The wing has an aspect ratio of unity and a chord of c = 69 mm. A right handed coordinate system (for the flow results) was defined with its origin at the intersection of the airfoil leading edge and flat plate, with x the stream-wise, y the span-wise, and z the crossflow directions respectively. The Reynolds number of the flow (based on chord length 69 mm and free steam velocity 38 m/s) was 1.75×10^5.

The flow was treated as incompressible and solved using the OpenFOAM code (Weller et al., 1998) using the Semi-Implicit Method for Pressure-Linked Equations algorithm. The RANS equations were solved using the realisable k-ε turbulence model for closure. The inlet boundary condition of the domain was set to be identical to that of a turbulent boundary layer with the same height as the airfoil chord. A no-slip boundary condition was applied to the floor and airfoil. The sides of the domain had zero-normal-gradient boundary conditions applied to them, while the roof was an inlet type boundary with a constant velocity equal to the free stream (38 m/s).

Linear interpolation schemes were used throughout, as was a second-order accurate linear scheme for the discretisation of gradient terms. The velocity field divergence terms were discretised using an interpolation scheme in which traditional linear-upwind and linear interpolation schemes are blended to stabilise solutions while maintaining second-order behaviour. The turbulent kinetic energy and dissipation fields divergence terms were discretised using a first-order accurate upwind scheme. All Laplacian terms were discretised with the second-order accurate linear scheme with explicit non-orthogonal correction. Finally, explicit non-orthogonal correction was performed when calculating surface-normal gradient terms.

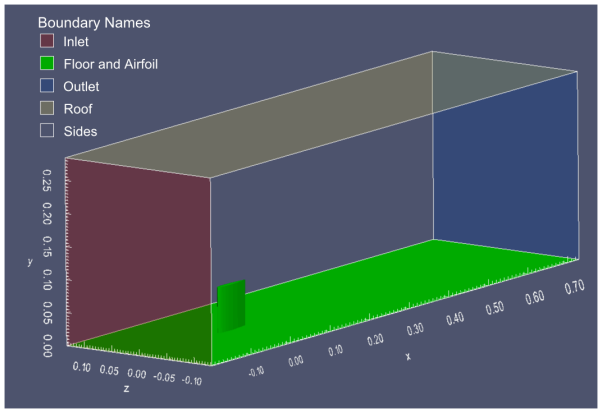

Figure 4. Computational domain. Flow is from lower left (Inlet) to upper right (Outlet). Units on axes are normalised by airfoil thickness T.

A grid refinement study was performed where the number of cells were increased until the flow solution became invariant and the drag coefficient changed by less than 1.05%. The final mesh used in this study contained 12,058,082 cells. The computations were performed on a 24-core workstation using the Linux operating system. The flow simulation required approximately one week of (wall-clock) time to produce a converged result.

Flow Results

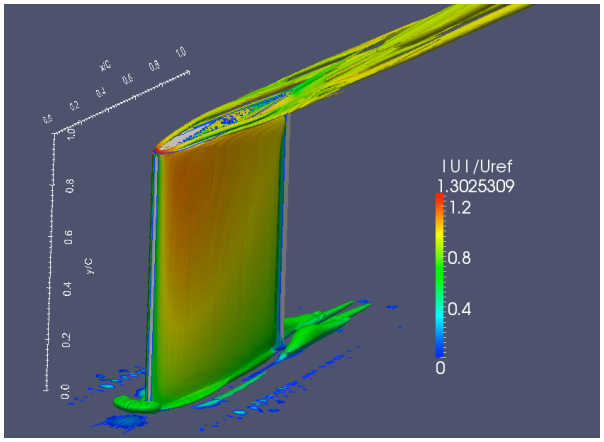

Figure 5. Iso-contours of the second invariant of the velocity gradient tensor Q about the wing-in-junction flow, coloured by velocity magnitude. Flow is from left to right.

The flow field about the wing-in-junction test case is summarised in Figure 5. Here and in the flow results that follow, the reference velocity used for non-dimensionalisation was set to $U_{ref} = 38$ m/s. In Figure 5, iso-contours of the flow parameter Q (the second invariant of the velocity gradient tensor, which is a scalar measure of the flow strain rate) show the main flow structures about the wing. At the junction of the wing and floor, a vortex forms around the leading edge of the wing. There is a trace of a trailing vortex structure along the chord at the base of the wing while large, well-defined structures are formed along the floor in the wake. Well-defined vortex structures form over the tip of wing and into the wake, which evolve and merge with additional trailing vortices to form a complex wake from the tip region.

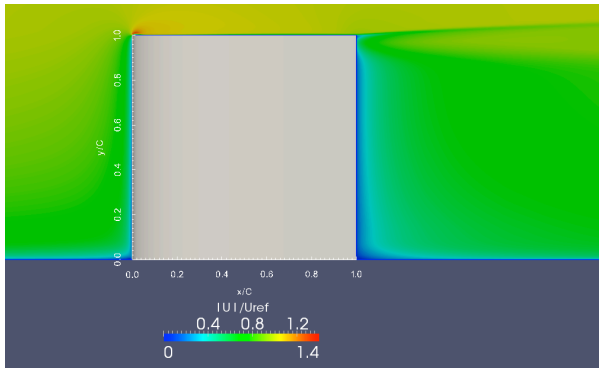

Figure 6. Contours of normalised velocity magnitude on the x-y plane at $z = 0$.

Figure 6 shows contours of computed normalised velocity magnitude on the x-y plane at $y = 0$. The computational data shows the flow impacting upon the leading edge, accelerating around the tip and expanding into the wake. Non-dimensionalised turbulent kinetic energy about the wing is shown in Figure 7. The turbulent kinetic energy is non-uniform upstream of the leading edge. Similarly, turbulent dissipation (Figure 8) is non-uniform upstream of the leading edge of the wing. Therefore, this variation in mean properties upstream of the leading edge must be taken into account when computing noise.

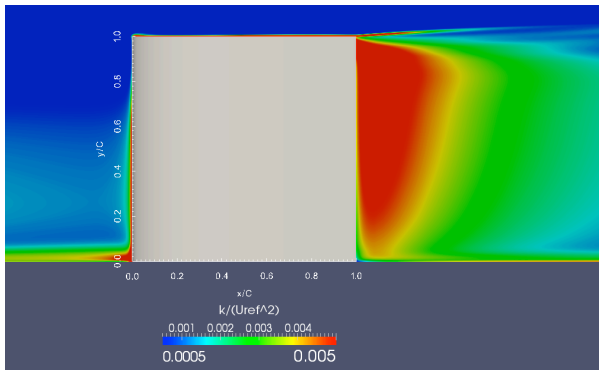

Figure 7. Contours of normalised turbulent kinetic energy on the x-y plane at $z = 0$.

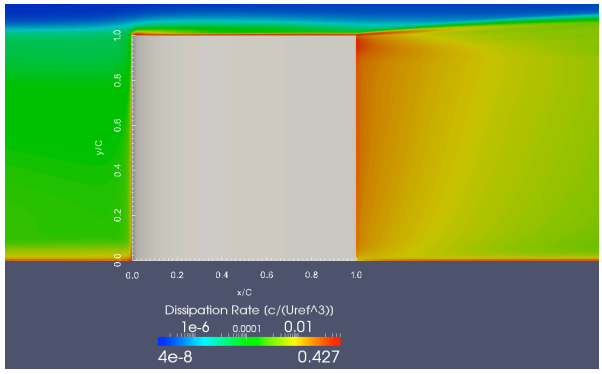

Figure 8. Contours of normalised turbulent dissipation on the x-y plane at $z = 0$.

Amiet's theory of leading-edge noise, used as a basis for the noise methodology presented here, is based on flow turbulence properties measured in the absence of an airfoil. That is, turbulence intensity and length scale are measured in a wind tunnel prior to the installation of a model. However,

the effect of solid surfaces will alter the turbulence intensity and dissipation in their close vicinity and care must be taken when collecting flow data upstream of the leading edge for noise calculations. In order to investigate this effect, data were collected at two locations upstream of the leading edge. These data are summarised in Figure 9 and will be discussed in the following paragraphs.

Data were collected along a line that extended from the floor to a position equal to the span of the airfoil at two stream-wise locations upstream of the leading edge. One location was chosen to be very close to the leading edge (x/c = -0.0032) where the flow is strongly influenced by the leading edge. The second location was chosen to be relatively far from the leading edge (x/c = -0.203) where the flow was unaffected by the wing and was similar to the flow entering the computational domain.

Figure 9(a) shows the mean stream-wise velocity profiles at the two stream-wise locations. The effect of the wing is obvious in this case. At the upstream location, the velocity profile resembles that of the inlet profile, which is a turbulent boundary layer. Close to the leading edge, the flow has slowed considerably and is no longer similar to that of a boundary layer.

In Figure 9(b) turbulent kinetic energy profiles are shown at the two stream-wise locations. In this case, the profiles are similar in shape, but the magnitude of the data close to the leading edge is higher than that computed upstream. This is because the turbulence model detects a wall and increases the production of turbulence to form a boundary layer. Even though the mean flow velocity is low, the turbulent kinetic energy is high, thus the overall effect of these competing parameters on noise generation is unclear without the use of an acoustic model. It is also interesting to note the production of what is termed here as a "secondary" shear layer along the floor of the domain upstream of the boundary layer. This is clearly identified in the computational data as a peak in the turbulent kinetic energy data over $0 \leq y/c \leq 0.1$. This region of higher turbulence intensity will produce more noise than would otherwise be expected from a flow without the secondary shear layer.

Figure 9(c) compares the turbulent dissipation at the leading edge and upstream from it. Similar to the turbulent kinetic energy results of Figure 9(b), dissipation is higher closer to the leading edge due to the high production of turbulence induced by the presence of the wall. The secondary shear layer is also noticeable in the dissipation results.

The turbulent kinetic energy profiles of Figure 9(b) were converted to turbulence intensity profiles using Equation (3), for use with the leading-edge noise model (Equation (5)). The results of this conversion are shown in Figure 9(d). The turbulence intensity profiles are identical in shape to the turbulent kinetic energy. The turbulence intensity is higher at the floor and varies in a non-uniform manner to the tip. Close to the leading edge, the effect of the wing tip is noticed in the results, where turbulence intensity increases as y/c approaches unity.

Turbulent integral length scale profiles were computed from the computational data and are shown in Figure 9(e). There are considerable differences between the two stream-wise locations and each will have a significant effect on the noise calculation.

Acoustic Results

Before the acoustic calculations can be performed, an understanding of the effect of span-wise discretisation must be obtained. The effect of the number of strips (N) on the root-mean-square (rms) of the predicted acoustic signal was investigated by calculating the power spectral density of the acoustic pressure from the wing-in-junction flow using Equation (5). In each case, the observer or virtual microphone location was placed at (x_a y_a z_a)= (0 0 600) mm directly over the centre of the wing surface (90 degrees to the chord line). For various values of N, the predicted spectrum was integrated over the frequency range of 100 Hz to 20 kHz to obtain an overall unweighted sound pressure level. The values of N used for this study were N = [1 5 50 100 500]. A value of N = 1 means that the span-wise varying flow upstream of the leading edge was averaged over the span. Similarly, $N > 1$ indicates that N equispaced strips were created, and the flow properties upstream of the leading edge were averaged over each strip and used in the acoustic calculation.

Figure 10 displays the results of the investigation of the effect of number of strips on acoustic prediction. The figure shows the percentage change in solution (the unweighted overall sound pressure level) versus number of strips using the numerical flow data taken at the upstream location (x/c = -0.203). The percentage change in solution was calculated by dividing change in the integrated pressure level from one solution to the next as N increased and expressing it as a percent. The acoustic solution is quite sensitive to the number of strips used when $N < 100$. However, when $N > 100$, the solution appears to be unaffected, indicating the numerical method has become grid insensitive and converged. Thus, the acoustic calculations presented here will use a value of N = 100, which corresponds to a strip width of dy = 0.69 mm for the wing-in-junction test case.

Predicted leading edge noise spectra are shown in Figure 11. These spectra were obtained using Equation (5) using the data presented in Figure 9 and at both stream-wise locations, i.e. those labelled "Upstream" (x/c = -0.203**)** and "Leading edge" (x/c = -0.0032). The results clearly show the importance of choosing the location to sample the in-coming flow correctly. The spectrum calculated using the leading edge (x/c = -0.0032) flow data is approximately 35 dB below the spectrum calculated using the upstream flow data (x/c = -0.203**)**. The reason for this discrepancy can be traced to differences in the mean flow data, specifically the differences in turbulent integral length scale (Figure 9(e)) and mean velocity (Figure 9(a)).

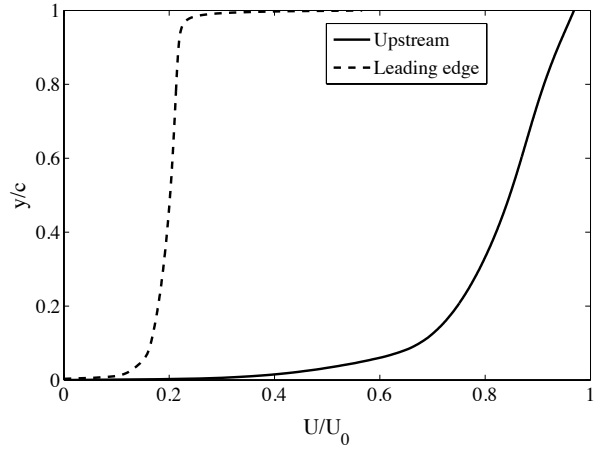

(a) Mean velocity

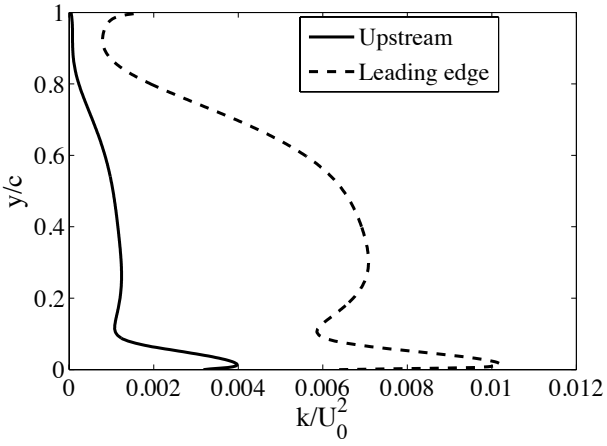

(b) Turbulent kinetic energy

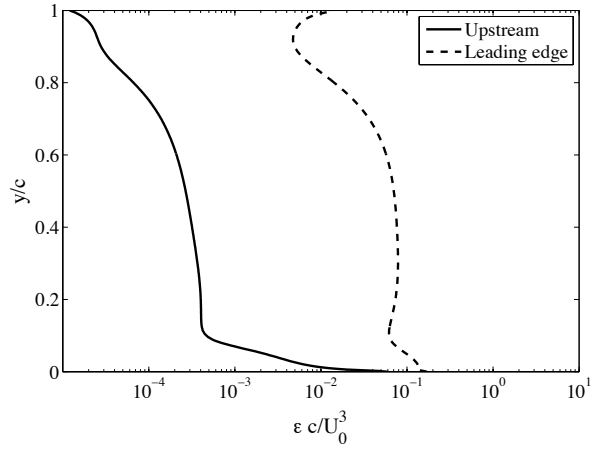

(c) Dissipation

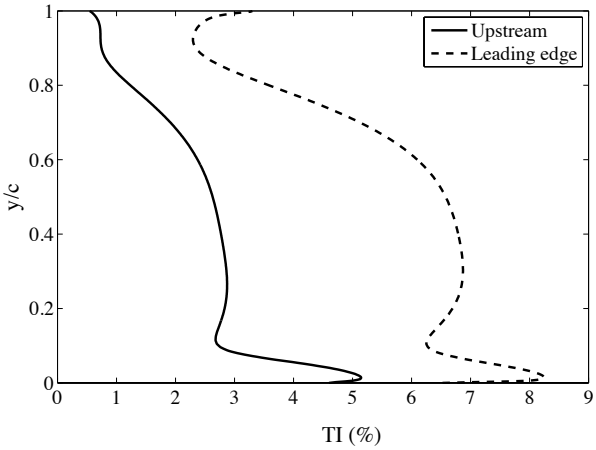

(d) Turbulence intensity

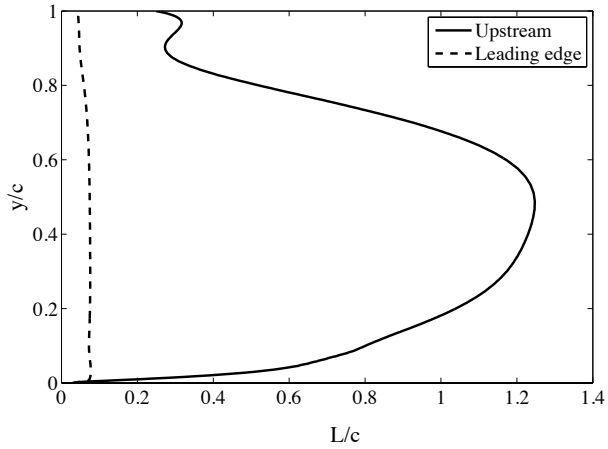

(e) Integral length scale

Figure 9. Flow property profiles measured upstream of the leading edge of the wing. Solid line (labelled "Upstream") indicates a position *x/c* = -0.203 upstream of the leading edge, at a position where the flow variables are unaffected by the presence of the wing; dashed line (labelled "Leading edge") indicates a position *x/c* = -0.0032 upstream of the leading edge.

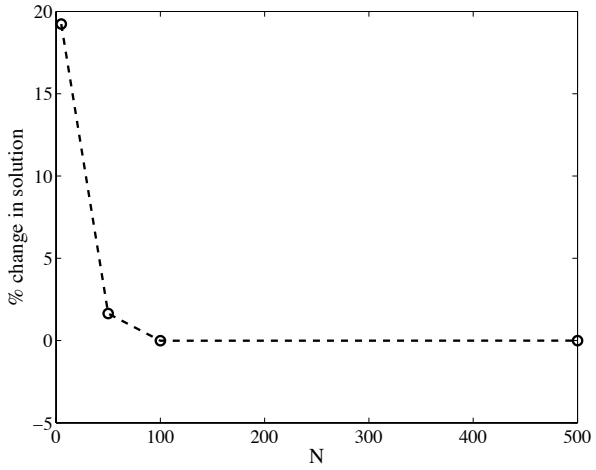

Figure 10. Effect of the number of strips (*N*) on the acoustic solution expressed as a percentage change in overall unweighted sound pressure level.

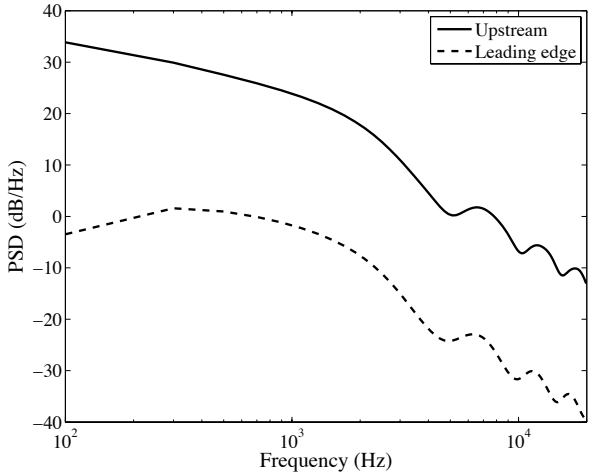

Figure 11. Comparison of acoustic power spectral densities (PSD) using numerical flow data from two upstream locations. Solid line (labelled "Upstream") indicates a position *x/c* = -0.203; Dashed line (labelled "Leading edge") indicates a position *x/c* = -0.0032.

Observing Equation (5), the sound pressure level (G_{pp}) is proportional to U^2 and the product of $\phi_{ww}(\omega)$ and $l_y(\omega)$, the turbulence velocity spectrum and span-wise turbulence correlation length scale, respectively. Both the turbulence spectrum and correlation length scale are functions of L (Amiet, 1975), resulting in acoustic pressure having an L^2 dependence. Hence, reductions in U and L will result in a large decrease in acoustic pressure in the far field. Note that turbulence intensity increases near the leading edge (Figure 9(d)), compared with the upstream location. As the turbulence velocity spectrum is only linearly related to turbulence intensity (Amiet, 1975), the increase due to this effect is small compared with the reduction due to velocity and turbulence length scale, hence the overall sound pressure level will reduce.

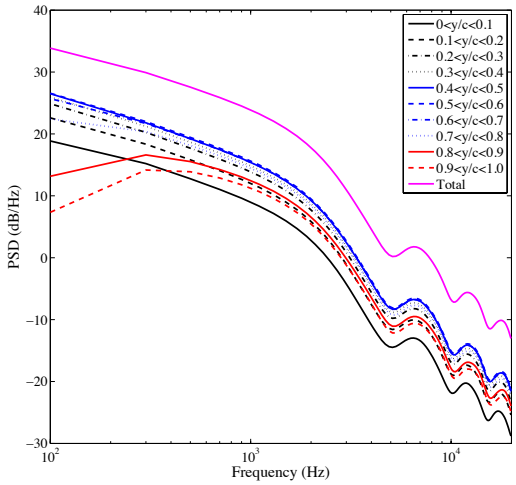

Figure 12. Prediction of acoustic power spectral density (PSD) for the wing-in-junction test case (Upstream) showing the contribution from sections of the span each of width equal to 10% of the chord.

Figure 12 shows the predicted acoustic power spectral density along with contributions from various sections of the span in order to link the flow physics to noise generation more directly. The span was divided into equal widths of 10% chord and acoustic power spectral density calculated for each. These data are shown in Figure 12 and are compared with the acoustic power spectral density for the entire wing (labelled "Total"). Most of the noise is being produced from the upper part of the wing, where $y/c > 0.5$. In this region of the flow field, the mean velocity is high and the turbulence length scales are large. As discussed earlier in this section, the radiated sound is very sensitive to these parameters and explains why the upper part of the wing is responsible for most of the noise generation. Thus, any noise control strategies for these types of flow should take this into consideration. When a boundary layer on a surface encounters an object connected to it, it is the flow in the upper region of the boundary layer that is responsible for most of the noise production. In the present case where the boundary layer is of the same height as the span, any noise mitigation strategies should involve either shape modifications or turbulence control in the upper region of the wing.

SUMMARY AND CONCLUSIONS

A leading edge noise model has been extended to include the effects of span-wise variations in flow properties as well as integration into RANS-based numerical flow solutions. The benefits of these extensions to the original leading edge noise model are that they can be used for modern engineering design that uses CFD methods to calculate the sometimes complex, non-uniform turbulent flows encountering airfoils.

The implementation of Amiet's leading edge noise model was validated successfully against some experimental data from the literature. The use of the extended leading edge model was demonstrated against a wing-in-junction flow test case as it contains complex non-uniform flow.

Predicted noise spectra were obtained using flow from two upstream locations to investigate the effect of the wing on the on-coming flow. As the noise model was originally derived using the undisturbed turbulence field as an input, it is ex-

pected that the noise results obtained using the upstream (*x/c* = -0.203**)** data will be closer to that expected in reality. However, this may not be the case and careful experimental measurements are needed to validate these predictions.

An investigation of the contribution of each part of the span to the far-field noise was performed. The upper 50% of the wing leading edge contributed most of the noise and this can be explained in terms of the flow properties. It is concluded that any noise mitigation strategies for wing-in-junction flows must concentrate on the upper regions of the boundary layer where flow velocity is high and integral turbulence lengths scales are large.

ACKNOWLEDGEMENTS

This work has been supported by the Australian Research Council under linkage grant LP110100033 'Understanding and predicting submarine hydrofoil noise'.

REFERENCES

Amiet, R. (1975) Acoustic radiation from an airfoil in a turbulent stream. *Journal of Sound and Vibration* 41, 407-420.

Curle, N. (1955) The influence of solid boundaries on aerodynamic sound. *Proc. Roy. Soc. London* A231, 505-514.

Doolan, C. J., Albarracin Gonzalez, C., & Hansen, C. H. (2010) Statistical estimation of turbulent trailing edge noise. *Proceedings of the 20th International Congress on Acoustics*, Sydney.

Moreau, D. J., Brooks, L. A., & Doolan, C. J. (2011) Broadband trailing edge noise from a sharp-edged strut. *The Journal of the Acoustical Society of America* 129, 2820-2829.

Paterson, R. & Amiet, R. (1982) Noise of a model helicopter rotor due to ingestion of isotropic turbulence. *Journal of Sound and Vibration* 85, 551-577.

Paterson, R. & Amiet, R. (1977) Noise and surface pressure response of an airfoil to incident turbulence. *J. Aircraft* 14, 729-736.

Pope, S. B. (2000) *Turbulent Flows*. Cambridge University Press, UK.

Roger, M. & Moreau, S. (2004) Broadband self-noise from loaded fan blades. *AIAA Journal* 42, 536--544.

Weller, H. G., Tabor, G., Jasak, H., & Fureby, C. (1998) A tensorial approach to CFD using object orientated techniques. *Computers in Physics* 12, 620-631.

Wilcox, D. C. (2006) *Turbulence Modeling for CFD*. DCW Industries, USA.